

# Is atmospheric oxidation capacity better in indicating tropospheric O<sub>3</sub> formation?

Peng Wang<sup>1,2</sup>, Shengqiang Zhu<sup>3</sup>, Mihalis Vrekoussis<sup>4,5</sup>, Guy P. Brasseur<sup>6,7</sup>, Shuxiao Wang (✉)<sup>8,9</sup>,  
Hongliang Zhang (✉)<sup>2,3,10</sup>

1 Department of Atmospheric and Oceanic Sciences, Fudan University, Shanghai 200438, China

2 IRDR ICoE on Risk Interconnectivity and Governance on Weather/Climate Extremes Impact and Public Health, Fudan University, Shanghai 200438, China

3 Shanghai Key Laboratory of Atmospheric Particle Pollution and Prevention, Department of Environmental Science & Engineering, Fudan University, Shanghai 200438, China

4 Institute of Environmental Physics, University of Bremen, Bremen D-28359, Germany

5 Climate and Atmosphere Research Center (CARE-C), the Cyprus Institute, Nicosia 27456, Cyprus

6 Max Planck Institute for Meteorology, Hamburg 20146, Germany

7 National Center for Atmospheric Research, Boulder, CO 80307, USA

8 State Key Joint Laboratory of Environmental Simulation and Pollution Control, School of Environment, Tsinghua University, Beijing 100084, China

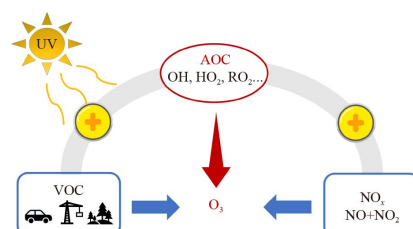
9 State Environmental Protection Key Laboratory of Sources and Control of Air Pollution Complex, Beijing 100084, China

10 Institute of Eco-Chongming (IEC), Shanghai 202162, China

## HIGHLIGHTS

- This study summarizes and evaluates different approaches that indicate O<sub>3</sub> formation.
- Isopleth and sensitivity methods are useful but have many prerequisites.
- AOC is a better indicator of photochemical reactions leading to O<sub>3</sub> formation.

## GRAPHIC ABSTRACT



## ABSTRACT

Tropospheric ozone (O<sub>3</sub>) concentration is increasing in China along with dramatic changes in precursor emissions and meteorological conditions, adversely affecting human health and ecosystems. O<sub>3</sub> is formed from the complex nonlinear photochemical reactions from nitrogen oxides (NO<sub>x</sub> = NO + NO<sub>2</sub>) and volatile organic compounds (VOCs). Although the mechanism of O<sub>3</sub> formation is rather clear, describing and analyzing its changes and formation potential at fine spatial and temporal resolution is still a challenge today. In this study, we briefly summarized and evaluated different approaches that indicate O<sub>3</sub> formation regimes. We identify that atmospheric oxidation capacity (AOC) is a better indicator of photochemical reactions leading to the formation of O<sub>3</sub> and other secondary pollutants. Results show that AOC has a prominent positive relationship to O<sub>3</sub> in the major city clusters in China, with a goodness of fit ( $R^2$ ) up to 0.6. This outcome provides a novel perspective in characterizing O<sub>3</sub> formation and has significant implications for formulating control strategies of secondary pollutants.

## ARTICLE INFO

### Article history:

Received 22 February 2022

Revised 8 April 2022

Accepted 10 April 2022

Available online 20 May 2022

### Keywords:

O<sub>3</sub>

AOC

O<sub>3</sub> formation regime

© Higher Education Press 2022

✉ Corresponding authors

E-mails: shxwang@tsinghua.edu.cn (S. Wang); zhanghl@fudan.edu.cn (H. Zhang)

Special Issue—Frontier Progresses from Chinese-American Professors of Environmental Engineering and Science (Responsible Editors: Xing Xie, Jinkai Xue & Hongliang Zhang)

## 1 Introduction

Tropospheric ozone ( $O_3$ ) is considered a key air pollutant that causes, among others, respiratory problems on humans and damages and reduced growth on plants (Lippmann, 1989; Chen et al., 2007; Feng and Kobayashi, 2009; Van Dingenen et al., 2009). It is mainly produced by photochemical reactions of volatile organic compounds (VOCs) and nitrogen oxides ( $NO_x$ ) from both natural and anthropogenic sources, although transport from the stratosphere is possible (Husain et al., 1977; Steinfeld, 1998).  $O_3$  and its precursors can be transported at great distances (Clarke and Ching, 1983; Lelieveld et al., 2009). Thus, its ambient level at a specific location is impacted by transported  $O_3$  from upwind sources and locally produced  $O_3$  through photochemical reactions.

$O_3$  formation occurs due to  $NO_2$  photolysis but formed  $O_3$  reacts with NO to regenerate  $NO_2$  without net  $O_3$  accumulation (Steinfeld, 1998). However,  $O_3$  accumulates when hydroperoxyl radical ( $HO_2$ ) or peroxy radicals ( $RO_2$ ) formed in VOCs oxidation by the hydroxyl radical ( $OH$ ) replace  $O_3$  in converting NO back to  $NO_2$  (Kentarchos and Roelofs, 2003; Pollack et al., 2013; Ren et al., 2013; Tan et al., 2018). Thus,  $O_3$  formation depends on the levels of  $NO_x$ , VOCs, and oxidants ( $OH$ ,  $HO_2$ , and  $RO_2$ , Fig. 1(a)). At different atmospheric conditions,  $O_3$  formation varies nonlinearly to different mixtures of  $NO_x$  and VOCs (Sillman et al., 1990; Sillman, 1999). In rural areas, where  $NO_x$  levels are usually low,  $O_3$  peak concentration decreases when  $NO_x$  is further reduced ( $NO_x$ -limited regime). Contrary, in urban areas, where  $NO_x$  amounts are elevated, a decrease in  $NO_x$  at constant VOC levels will increase  $O_3$  peak concentrations (VOC-limited regime). Following this methodology,  $O_3$  formation is usually split into VOC-limited regime,  $NO_x$ -limited regime, and transition regime that governing by both  $NO_x$  and VOCs (Sillman, 1995; Sillman and He, 2002). Numerical studies have focused on identifying  $O_3$  formation regimes for designing controlling strategies (Feng et al., 2016; Ye et al., 2016;

Lu et al., 2019; Wang et al., 2019b). Xing et al. (2011) investigated the nonlinear response of  $O_3$  to precursor emission changes in China and found that  $NO_x$  control appears to be beneficial for  $O_3$  reduction in the downwind areas which usually experience high  $O_3$  levels. Jin and Holloway (2015) investigated the  $O_3$  sensitivity regime from 2005 to 2013 in China. They found that reducing  $NO_x$  emissions is an effective way to control  $O_3$  pollution in the Pearl River Delta (PRD). Wang et al. (2019a) reported that the  $O_3$  sensitivity turned into a transition regime in eastern China in recent years, which required more comprehensive emissions control strategies to alleviate  $O_3$  better. Ding et al. (2022) highlighted the necessity of simultaneous VOCs and  $NO_x$  emission control in winter while enhancing the  $NO_x$  control in the summer. However, most of these studies neglected the importance of atmospheric oxidation capacity (AOC) as the formation regimes are changing. The AOC is a key factor that describes  $O_3$  formation (Kentarchos and Roelofs, 2003; Prinn, 2003; Li et al., 2019b). Generally, AOC is defined as the total oxidation reaction rates of primary pollutants (such as VOCs) by the oxidants (e.g.  $OH$ ,  $HO_2$ , and  $NO_3$ ). And the concentrations of these oxidants are used as an indicator to assess the AOC level in the modeling studies. Regardless of the changes in the regime and emissions of  $NO_x$  and VOCs, faster reaction rates, indicated by higher levels of oxidants, would lead to enhanced  $O_3$  formation. The following question is then posed: Which is a better indicator when assessing  $O_3$  formation. Here, we discuss different ways to understand  $O_3$  formation and propose that AOC should be additionally considered when designing control policies.

## 2 Isopleth diagram

As mentioned before, an  $O_3$  isopleth diagram is defined as a contour plot of interpolated maximum  $O_3$  concentrations achieved as a function of VOC and  $NO_x$  concentrations (Dodge, 1977). It is used to show the

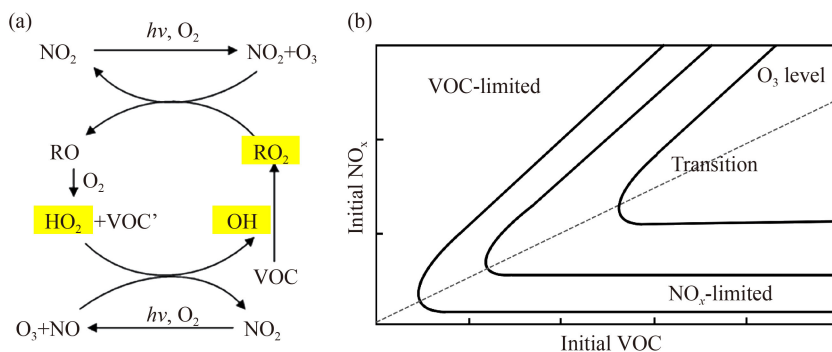


**Fig. 1** (a) The  $O_3$  formation mechanism (highlighted parts are the major oxidants) modified from Steinfeld (1998) and (b) a typical  $O_3$  isopleth.

degree of O<sub>3</sub> production by considering the relative abundances of NO<sub>x</sub> and VOCs, including constant VOCs composition and meteorological conditions (Milford et al., 1989; Jin and Demerjian, 1993; Menut et al., 2000). These isopleths provide characteristic O<sub>3</sub> ridgelines, which depict the maximum achievable O<sub>3</sub> concentration at the NO<sub>x</sub>-limited, VOC-limited and transition regimes (Fig. 1(b)).

O<sub>3</sub> isopleth plots are widely used as a key methodology applied in O<sub>3</sub> control strategies. However, some complex prerequisites are required when interrelating the isopleths. To generate these plots, O<sub>3</sub> maximum concentration has to be predicted from a large number of numerical simulations performed with an atmospheric VOC/NO<sub>x</sub> chemical mechanism using varying initial concentrations of VOCs and NO<sub>x</sub>. At the same time, all other variables are constant (Qian et al., 2019). In short, the following points need to be considered when interrelating O<sub>3</sub> isopleths:

- 1) A large amount of simulations is required to plot the isopleth;
- 2) The correlation of O<sub>3</sub> with NO<sub>x</sub> and VOCs varies greatly on the different assumptions and conditions (such as meterological parameters), which is partly due to complex atmospheric processes such as regional transport;
- 3) The computation of isopleths is based on constant VOCs composition; however, ambient VOCs composition may vary in time as its total concentration changes;
- 4) Biogenic VOCs (BVOCs) are not considered in most cases as they are not controllable, although they represent a significant fraction of the total VOC budget, especially in suburban and rural areas;
- 5) There are no prescribed common conditions for determining O<sub>3</sub> formation regimes using the isopleths since they depend on multiple factors such as emission inventories, chemical mechanisms, and meteorological conditions;
- 6) Since the isopleths may encoushicnter temporal variability (day-by-day changes), the methodology has limitations to represent a persistent O<sub>3</sub> pollution episode that lasts for several days.

### 3 Sensitivity methods

State-of-the-art chemical transport models (CTM) are also used to provide sensitivity analysis methods to identify O<sub>3</sub> formation regimes (Sillman et al., 1990). Thereby, NO<sub>x</sub> or VOCs are reduced or increased by a certain percentage. Then, the simulated O<sub>3</sub> concentrations are compared with the base case (without NO<sub>x</sub> and VOCs changes). A certain difference (e.g. of 5 ppb) is used as a criterion to verify if O<sub>3</sub> formation is sensitive to NO<sub>x</sub> or VOCs reduction. In sensitivity methods, NO<sub>x</sub>-VOCs indicators from model prediction and ambient

measurements are often used to split O<sub>3</sub> formation to different regimes, which involve secondary species produced concurrently with photochemical O<sub>3</sub> production (Sillman, 1995, 1999; Sillman and He, 2002). These species are relatively long-lived, so they can be transported along with O<sub>3</sub>, including peroxydes (e.g. H<sub>2</sub>O<sub>2</sub>), nitric acid (HNO<sub>3</sub>), total reactive nitrogen (NO<sub>y</sub> = NO<sub>x</sub> + HNO<sub>3</sub> + peroxyacetyl nitrates + alkyl nitrates), and NO<sub>x</sub> reaction products (NO<sub>z</sub> = NO<sub>y</sub> - NO<sub>x</sub>). The ratios among these species reveal information associated with O<sub>3</sub> formation chemistry. The purpose of deriving these indicators is to build a link of O<sub>3</sub>-NO<sub>x</sub>-VOC to reduce the peak O<sub>3</sub> by the controllable species. The widely used indicators include, but are not limited to, VOCs/NO<sub>x</sub>, H<sub>2</sub>O<sub>2</sub>/NO<sub>y</sub>, H<sub>2</sub>O<sub>2</sub>/NO<sub>z</sub>, H<sub>2</sub>O<sub>2</sub>/HNO<sub>3</sub>, O<sub>3</sub>/HNO<sub>3</sub>, O<sub>3</sub>/NO<sub>y</sub>, and O<sub>3</sub>/NO<sub>z</sub>. Also, productions rates are often used to calculate O<sub>3</sub> formation regimes, such as (P<sub>H<sub>2</sub>O<sub>2</sub></sub> + P<sub>ROOH</sub>)/P<sub>HNO<sub>3</sub></sub> and P<sub>H<sub>2</sub>O<sub>2</sub></sub>/P<sub>HNO<sub>3</sub></sub> based on the production rates of H<sub>2</sub>O<sub>2</sub>, HNO<sub>3</sub>, and organic hydroperoxides (ROOH). Some of these indicators are derived from routinely monitored pollutants (e.g. O<sub>3</sub>) at observation sites or satellite retrievals (e.g. HCHO and NO<sub>2</sub>). Although the above mentioned indicators can be calculated directly from model simulations or satellite data, they are not probing into the complex reactions leading to O<sub>3</sub> formation and having uncertainties in indentifying O<sub>3</sub> formation regimes.

In practical implementation, using these indicators to evaluate the O<sub>3</sub> formation regimes requires extensive measurement networks (Jin and Holloway, 2015). Also, results from these indicators should be evaluated separately on a daily even hourly basis, especially for specific hours such as noon to two hours before sunset to maintain effectiveness. Even all these prerequisites are met, the NO<sub>x</sub>-VOCs indicators method may have limitations in understanding O<sub>3</sub> changes or identifying O<sub>3</sub> formation regimes when NO<sub>x</sub> or VOCs emissions are dramatically changed. For instance, during the COVID-19, O<sub>3</sub> concentrations in norther China increased when large emission reductions occurred due to reduced human activities during the lockdown (Gaubert et al., 2021; Zhu et al., 2021). One potential reason for this change was a shift in the O<sub>3</sub> formation regime due to the reduction in NO<sub>x</sub> emissions during the imposed lockdown (Wang et al., 2021b). However, this was concluded mainly based on indicators or isopleth analysis, which may not reflect reality accurately. In particular, during the COVID-19, the O<sub>3</sub> formation regime changed from VOC-limited to NO<sub>x</sub>-limted or transition regimes, but the rising O<sub>3</sub> concentrations were found with the NO<sub>x</sub> reduction. Table 1 shows the ratios of grid cells attributed to the three O<sub>3</sub> formation regimes (NO<sub>x</sub>-limited, VOC-limited and transition) during the COVID-19 lockdown (January and February 2020) under different precursors reductions in China. These regimes are calculated using the Community Multi-scale Air Quality (CMAQ) model.

**Table 1** Ratios of grid cells falling in different  $O_3$  formation regimes (VOC-limited,  $NO_x$ -limited, and transition regimes) suggested by three different indicators during COVID-19 lockdown (January and February 2020) under different precursors reductions cases. All results are calculated using Community Multi-scale Air Quality (CMAQ) model

Scenarios	Indicators	VOC-limited	$NO_x$ -limited	Transition
During COVID-19	$HCHO/NO_2$	0.13	0.70	0.17
	$O_3/NO_y$	0.11	0.40	0.49
	$H_2O_2/NO_y$	0.42	0.15	0.43
VOCs reduced by 50%	$HCHO/NO_2$	0.19	0.65	0.16
	$O_3/NO_y$	0.14	0.39	0.47
	$H_2O_2/NO_y$	0.42	0.15	0.43
$NO_x$ reduced by 50%	$HCHO/NO_2$	0.02	0.85	0.13
	$O_3/NO_y$	0.03	0.51	0.46
	$H_2O_2/NO_y$	0.24	0.19	0.57
VOCs and $NO_x$ reduced by 50%	$HCHO/NO_2$	0.04	0.79	0.17
	$O_3/NO_y$	0.03	0.52	0.45
	$H_2O_2/NO_y$	0.25	0.19	0.56

Details on the simulation and analysis can be found in Zhu et al. (2021). It is evident that the depending on the selected indicators different results are produced when identifying  $O_3$  formation regimes. The  $HCHO/NO_2$  indicator predicts a higher percentage of grids for the  $NO_x$ -limited regime and the  $O_3/NO_y$  predicts more for the transition one. Contrary, the  $H_2O_2/NO_y$  favors the VOCs-limited regime. In addition, these three indicators show different sensitivities when changes (reductions) in  $O_3$  precursors species emissions are considered. When the VOC emissions decrease by 50%, there are no changes in the formation regimes indicated by the  $H_2O_2/NO_y$  ratio. In contrast, an enhancement of the grid percentage corresponding to the VOC-limited regime (~46% increasing rate) is predicted using the  $HCHO/NO_2$  ratio. Consequently, different conclusions can be reached using different indicators.

#### 4 Atmospheric oxidation capacity (AOC)

Reassessing its formation mechanism,  $O_3$  is formed through photochemical reactions. The overall processes are related to the atmospheric oxidation capacity (AOC), which can be characterized by the levels of atmospheric oxidants, mainly including hydrogen oxide radicals ( $HO_x = OH + HO_2$ ) during daytime, and nitrogen oxide radical ( $NO_3$ ) (Jacob, 2000; Monks, 2005) during nighttime. There are also other approaches to define the AOC. Elshorbany et al. (2009) identified the AOC as the sum of the explicit oxidation rates of primary pollutants by the oxidants. Liu et al. (2021) calculated the AOC based on electron transfer during the secondary pollutants formation process. The AOC is a fundamental factor in understanding the formation of  $O_3$  and other secondary species. Despite its potential, only a handful of

studies reported the importance of AOC in explaining changes in  $O_3$  formation in China. Li et al. (2019a) found that since 2013, high AOC along with  $PM_{2.5}$  reductions is the reason for the reported  $O_3$  increases in China. Since the  $PM_{2.5}$  is considered as the sink of the  $HO_x$  (a major component of AOC), its reduction leads to the increase of AOC. Wang et al. (2021c) and Zhu et al. (2021) also reported that the unexpectedly rising amounts of  $O_3$  during the COVID-19 were mainly attributed to the enhanced AOC since they had similar variation trends and spatial distributions.

Herewith, we aim at better understanding the interplay between AOC and  $O_3$  formation. Among all oxidants,  $HO_x$  concentrations are related to  $O_3$  formation significantly, and even their day-to-day co-variations have been noticed in different cities and episodes (Porter et al., 2017; Chen et al., 2020; Zhu et al., 2020). Zhao et al. (2021) reported that the average day-to-day co-variations between  $HO_x$  and  $O_3$  is larger than 0.55 in the PRD. However, there is no further evidence in the relationships between AOC with  $O_3$  concentrations and changes in  $O_3$  concentrations. As a very preliminary test, the results from COVID-19 periods are summarized. Table 2 shows the correlations between the  $HO_x$  and  $O_3$  in the major city clusters, including the North China Plain (NCP), the Yangtze River Delta (YRD), and the PRD in China during the COVID-19 (January and February, 2020).  $O_3$  from biogenic source is also considered, since recent studies reported that the BVOCs played an important role in the city clusters due to the urban greening impacts (Ma et al., 2019; Ma et al., 2022). In general, there is a significant positive correlation between non-background  $O_3$  and  $HO_x$  in all these three regions. The maximum goodness of fit ( $R$ ) is predicted for the NCP ( $R^2 = 0.47$ ) where, the most significant increase of  $O_3$  (average increase rate ~54%) was reported (Zhu et al.,

**Table 2** The correlation between HO<sub>x</sub> and non-background (NB) O<sub>3</sub> and O<sub>3</sub> in the major city clusters (NCP, YRD and PRD regions) in China during COVID-19 under different emission control conditions. The NB O<sub>3</sub> is the sum of O<sub>3</sub> from all emission sources (including both anthropogenic and biogenic sources). Units for NB O<sub>3</sub>/O<sub>3</sub> and HO<sub>x</sub> are ppb and ppt. Total grid cells are 284, 277, and 158 in the NCP, YRD, and PRD, respectively. Total data points are 10508, 10247, and 5846 in the NCP, YRD, and PRD, respectively

NB	NCP	YRD	PRD
O <sub>3</sub>			
During COVID-19	O <sub>3</sub> = 3.7*HO <sub>x</sub> +0.2, R <sup>2</sup> = 0.47	O <sub>3</sub> = 1.8*HO <sub>x</sub> +0.6, R <sup>2</sup> = 0.40	O <sub>3</sub> = 1.2*HO <sub>x</sub> +1.6, R <sup>2</sup> = 0.27
During COVID-19	O <sub>3</sub> = 2.1*HO <sub>x</sub> +0.9, R <sup>2</sup> = 0.42	O <sub>3</sub> = 2.7*HO <sub>x</sub> -4.0, R <sup>2</sup> = 0.60	O <sub>3</sub> = 2.7*HO <sub>x</sub> -7.2, R <sup>2</sup> = 0.43
NO <sub>x</sub> reduced by 50%	O <sub>3</sub> = 1.5*HO <sub>x</sub> +0.7, R <sup>2</sup> = 0.49	O <sub>3</sub> = 2.2*HO <sub>x</sub> -6.4, R <sup>2</sup> = 0.03	O <sub>3</sub> = 2.0*HO <sub>x</sub> -9.2, R <sup>2</sup> = 0.55
VOCs reduced by 50%	O <sub>3</sub> = 1.3*HO <sub>x</sub> +0.7, R <sup>2</sup> = 0.14	O <sub>3</sub> = 2.8*HO <sub>x</sub> -3.4, R <sup>2</sup> = 0.39	O <sub>3</sub> = 1.9*HO <sub>x</sub> -7.0, R <sup>2</sup> = 0.05
VOCs and NO <sub>x</sub> reduced by 50%	O <sub>3</sub> = 1.2*HO <sub>x</sub> +0.6, R <sup>2</sup> = 0.29	O <sub>3</sub> = 2.8*HO <sub>x</sub> -6.5, R <sup>2</sup> = 0.69	O <sub>3</sub> = 2.3*HO <sub>x</sub> -8.9, R <sup>2</sup> = 0.46

2021). In addition, O<sub>3</sub> concentrations also show high sensitivity to the changes of AOC (average increase rate ~98%) in the NCP, represented by the higher regression slope (slope = 3.7). Compared to the NCP, the correlation is less strong ( $R^2 = 0.27$ ) for the PRD. The latter is consistent with the findings of previous studies denoting that O<sub>3</sub> concentration remained almost constant during the COVID-19 (Wang et al., 2021a; Zhu et al., 2021). Considering O<sub>3</sub> concentrations (sum of background and non-background O<sub>3</sub>), the positive correlations between it and AOC are even more significant with the  $R^2$  up to 0.60 in the YRD during COVID-19 (Table 2). Besides, previous studies also reported that the elevated O<sub>3</sub> was corresponding to the enhanced AOC during the summertime (Li et al., 2019a; Qin et al., 2022), indicating that the AOC may be a better indicator to elucidate the O<sub>3</sub> formation. However, these correlations vary greatly under different emission control strategies in different regions. In the YRD, the  $R^2$  drops from 0.6 to 0.03 when NO<sub>x</sub> emissions are reduced by 50%. While in the PRD, the  $R^2$  value is more sensitive to VOC decreases (from 0.43 to 0.05). The AOC levels highly depend on the meteorological parameters and emission conditions. Thus, the correlation between O<sub>3</sub> and AOC changes accordingly to the variations in meteorology and emissions. More comprehensive simulations are required to determine their relationships better under different emissions control scenarios.

## 5 Summary

In this study, we briefly summarized and evaluated the different methods for indicating the formation of tropospheric O<sub>3</sub>. The isopleth diagram and the sensitivity method are two widely used ways to describe O<sub>3</sub> formation. However, both require numerous simulations and the development of complex chemical mechanisms. In addition, they are also affected by multiple environmental factors, which leads to large uncertainties in policymaking decisions. The AOC is regarded as the fundamental factor in the formation of O<sub>3</sub> and other

secondary pollutants in the atmosphere. We suggest that the AOC could serve as a better indicator to characterize O<sub>3</sub> formation. Our results show that AOC and O<sub>3</sub> have a coincident variation trend in key city clusters (NCP, YRD, and PRD regions) in China and the average  $R^2$  between O<sub>3</sub> and AOC is as high as 0.60. As the AOC level could be determined as the sum of the major oxidants, it is important to figure out the budget (generation and remove processes) of these oxidants and then alleviate O<sub>3</sub> pollution via control the key precursors in their generation process. In addition, feasible control strategies should be considered under different meteorological conditions, since AOC highly depend on the meterological parameters such as temperature. More comprehensive studies should be conducted to investigate the variability of the correlation between O<sub>3</sub> and AOC with the ultimate aim of establishing effective emission control policies in the future.

**Acknowledgements** This work was supported by the co-funded DFG-NSFC Sino-German Air Changes Project (No. 448720203), the National Natural Science Foundation of China (Nos. 42077194/42061134008/42022023/92044302), and the Shanghai International Science and Technology Partnership Project (China) (No. 21230780200).

## References

- Chen S, Wang H, Lu K, Zeng L, Hu M, Zhang Y (2020). The trend of surface ozone in Beijing from 2013 to 2019: Indications of the persisting strong atmospheric oxidation capacity. *Atmospheric Environment*, 242: 117801
- Chen T M, Kuschner W G, Gokhale J, Shofer S (2007). Outdoor air pollution: Ozone health effects. *American Journal of the Medical Sciences*, 333(4): 244–248
- Clarke J F, Ching J K S (1983). Aircraft observations of regional transport of ozone in the northeastern United States. *Atmospheric Environment* (1967), 17(9): 1703–1712
- Ding D, Xing J, Wang S, Dong Z, Zhang F, Liu S, Hao J (2022). Optimization of a NO<sub>x</sub> and VOC cooperative control strategy based on clean air benefits. *Environmental Science & Technology*, 56(2): 739–749
- Dodge M (1977). Combined Use of Modeling Techniques and Smog

- Chamber Data to Derive Ozone-precursor Relationships, US Environmental Protection Agency. Research Triangle Park, North Carolina: US Environmental Protection Agency, 881–889
- Elshorbany Y F, Kurtenbach R, Wiesen P, Lissi E, Rubio M, Villena G, Gramsch E, Rickard A R, Pilling M J, Kleffmann J (2009). Oxidation capacity of the city air of Santiago, Chile. *Atmospheric Chemistry and Physics*, 9(6): 2257–2273
- Feng T, Bei N, Huang R J, Cao J, Zhang Q, Zhou W, Tie X, Liu S, Zhang T, Su X, Lei W, Molina L T, Li G (2016). Summertime ozone formation in Xi'an and surrounding areas, China. *Atmospheric Chemistry and Physics*, 16(7): 4323–4342
- Feng Z, Kobayashi K (2009). Assessing the impacts of current and future concentrations of surface ozone on crop yield with meta-analysis. *Atmospheric Environment*, 43(8): 1510–1519
- Gaubert B, Bouarar I, Doumbia T, Liu Y, Stavrakou T, Deroubaix A, Darras S, Elguindi N, Granier C, Lacey F, Müller J F, Shi X, Tilmes S, Wang T, Brasseur G P (2021). Global changes in secondary atmospheric pollutants during the 2020 COVID-19 pandemic. *Journal of Geophysical Research: Atmospheres*, 126(8): e2020JD034213
- Husain L, Coffey P E, Meyers R E, Cederwall R T (1977). Ozone transport from stratosphere to troposphere. *Geophysical Research Letters*, 4(9): 363–365
- Jacob D J (2000). Heterogeneous chemistry and tropospheric ozone. *Atmospheric Environment*, 34(12): 2131–2159
- Jin S, Demerjian K (1993). A photochemical box model for urban air quality study. *Atmospheric Environment. Part B, Urban Atmosphere*, 27(4): 371–387
- Jin X, Holloway T (2015). Spatial and temporal variability of ozone sensitivity over China observed from the ozone monitoring instrument. *Journal of Geophysical Research. Atmospheres*, 120(14): 7229–7246
- Kentarchos A S, Roelofs G J (2003). A model study of stratospheric ozone in the troposphere and its contribution to tropospheric OH formation. *Journal of Geophysical Research*, 108(D12): 8517
- Lelieveld J, Hoor P, Jöckel P, Pozzer A, Hadjinicolaou P, Cammas J P, Beirle S (2009). Severe ozone air pollution in the Persian Gulf region. *Atmospheric Chemistry and Physics*, 9(4): 1393–1406
- Li K, Jacob D J, Liao H, Shen L, Zhang Q, Bates K H (2019a). Anthropogenic drivers of 2013–2017 trends in summer surface ozone in China. *Proceedings of the National Academy of Sciences of the United States of America*, 116(2): 422–427
- Li K, Jacob D J, Liao H, Zhu J, Shah V, Shen L, Bates K H, Zhang Q, Zhai S (2019b). A two-pollutant strategy for improving ozone and particulate air quality in China. *Nature Geoscience*, 12(11): 906–910
- Lippmann M (1989). Health effects of ozone a critical review. *JAPCA*, 39(5): 672–695
- Liu Z, Wang Y, Hu B, Lu K, Tang G, Ji D, Yang X, Gao W, Xie Y, Liu J, Yao D, Yang Y, Zhang Y (2021). Elucidating the quantitative characterization of atmospheric oxidation capacity in Beijing, China. *Science of the Total Environment*, 771: 145306
- Lu H, Lyu X, Cheng H, Ling Z, Guo H (2019). Overview on the spatial-temporal characteristics of the ozone formation regime in China. *Environmental Science. Processes & Impacts*, 21(6): 916–929
- Ma M, Gao Y, Ding A, Su H, Liao H, Wang S, Wang X, Zhao B, Zhang S, Fu P, Guenther A B, Wang M, Li S, Chu B, Yao X, Gao H (2022). Development and assessment of a high-resolution biogenic emission inventory from urban green spaces in China. *Environmental Science & Technology*, 56(1): 175–184
- Ma M, Gao Y, Wang Y, Zhang S, Leung L R, Liu C, Wang S, Zhao B, Chang X, Su H, Zhang T, Sheng L, Yao X, Gao H (2019). Substantial ozone enhancement over the North China Plain from increased biogenic emissions due to heat waves and land cover in summer 2017. *Atmospheric Chemistry and Physics*, 19(19): 12195–12207
- Menut L, Vautard R, Beekmann M, Honoré C (2000). Sensitivity of photochemical pollution using the adjoint of a simplified chemistry-transport model. *Journal of Geophysical Research*, 105(D12): 15379–15402
- Milford J B, Russell A G, Mcrae G J (1989). A new approach to photochemical pollution control: Implications of spatial patterns in pollutant responses to reductions in nitrogen oxides and reactive organic gas emissions. *Environmental Science & Technology*, 23(10): 1290–1301
- Monks P S (2005). Gas-phase radical chemistry in the troposphere. *Chemical Society Reviews*, 34(5): 376–395
- Pollack I B, Ryerson T B, Trainer M, Neuman J A, Roberts J M, Parrish D D (2013). Trends in ozone, its precursors, and related secondary oxidation products in Los Angeles, California: A synthesis of measurements from 1960 to 2010. *Journal of Geophysical Research. Atmospheres*, 118(11): 5893–5911
- Porter W C, Safieddine S A, Heald C L (2017). Impact of aromatics and monoterpenes on simulated tropospheric ozone and total OH reactivity. *Atmospheric Environment*, 169: 250–257
- Prinn R G (2003). The cleansing capacity of the atmosphere. *Annual Review of Environment and Resources*, 28(1): 29–57
- Qian Y, Henneman L R F, Mulholland J A, Russell A G (2019). Empirical development of ozone isopleths: Applications to Los Angeles. *Environmental Science & Technology Letters*, 6(5): 294–299
- Qin M, Hu A, Mao J, Li X, Sheng L, Sun J, Li J, Wang X, Zhang Y, Hu J (2022). PM<sub>2.5</sub> and O<sub>3</sub> relationships affected by the atmospheric oxidizing capacity in the Yangtze River Delta, China. *Science of the Total Environment*, 810: 152268
- Ren X, Van Duin D, Cazorla M, Chen S, Mao J, Zhang L, Brune W H, Flynn J H, Grossberg N, Lefer B L, Rappenglück B, Wong K W, Tsai C, Stutz J, Dibb J E, Thomas Jobson B, Luke W T, Kelley P (2013). Atmospheric oxidation chemistry and ozone production: Results from SHARP 2009 in Houston, Texas. *Journal of Geophysical Research. Atmospheres*, 118(11): 5770–5780
- Sillman S (1995). The use of NO<sub>y</sub>, H<sub>2</sub>O<sub>2</sub>, and HNO<sub>3</sub> as indicators for ozone-NO<sub>x</sub>-hydrocarbon sensitivity in urban locations. *Journal of Geophysical Research*, 100(D7): 14175–14188
- Sillman S (1999). The relation between ozone, NO<sub>x</sub> and hydrocarbons in urban and polluted rural environments. *Atmospheric Environment*, 33(12): 1821–1845
- Sillman S, He D (2002). Some theoretical results concerning O<sub>3</sub>-NO<sub>x</sub>-VOC chemistry and NO<sub>x</sub>-VOC indicators. *Journal of Geophysical Research: Atmospheres*, 107(D22): ACH 26–21-ACH 26–15
- Sillman S, Logan J A, Wofsy S C (1990). The sensitivity of ozone to

- nitrogen oxides and hydrocarbons in regional ozone episodes. *Journal of Geophysical Research*, 95(D2): 1837–1851
- Steinfeld J I (1998). Atmospheric chemistry and physics: from air pollution to climate change. *Environment*, 40(7): 26
- Tan Z, Lu K, Jiang M, Su R, Dong H, Zeng L, Xie S, Tan Q, Zhang Y (2018). Exploring ozone pollution in Chengdu, southwestern China: A case study from radical chemistry to O<sub>3</sub>-VOC-NO<sub>x</sub> sensitivity. *Science of the Total Environment*, 636: 775–786
- Van Dingenen R, Dentener F J, Raes F, Krol M C, Emberson L, Cofala J (2009). The global impact of ozone on agricultural crop yields under current and future air quality legislation. *Atmospheric Environment*, 43(3): 604–618
- Wang N, Lyu X, Deng X, Huang X, Jiang F, Ding A (2019a). Aggravating O<sub>3</sub> pollution due to NO<sub>x</sub> emission control in eastern China. *Science of the Total Environment*, 677: 732–744
- Wang P, Chen Y, Hu J, Zhang H, Ying Q (2019b). Attribution of tropospheric ozone to NO<sub>x</sub> and VOC emissions: Considering ozone formation in the transition regime. *Environmental Science & Technology*, 53(3): 1404–1412
- Wang S, Zhang Y, Ma J, Zhu S, Shen J, Wang P, Zhang H (2021a). Responses of decline in air pollution and recovery associated with COVID-19 lockdown in the Pearl River Delta. *Science of the Total Environment*, 756: 143868
- Wang W, Van Der A R, Ding J, Van Weele M, Cheng T (2021b). Spatial and temporal changes of the ozone sensitivity in China based on satellite and ground-based observations. *Atmospheric Chemistry and Physics*, 21(9): 7253–7269
- Wang Y, Zhu S, Ma J, Shen J, Wang P, Wang P, Zhang H (2021c). Enhanced atmospheric oxidation capacity and associated ozone increases during COVID-19 lockdown in the Yangtze River Delta. *Science of the Total Environment*, 768: 144796
- Xing J, Wang S X, Jang C, Zhu Y, Hao J M (2011). Nonlinear response of ozone to precursor emission changes in China: A modeling study using response surface methodology. *Atmospheric Chemistry and Physics*, 11(10): 5027–5044
- Ye L, Wang X, Fan S, Chen W, Chang M, Zhou S, Wu Z, Fan Q (2016). Photochemical indicators of ozone sensitivity: Application in the Pearl River Delta, China. *Frontiers of Environmental Science & Engineering*, 10(6): 15
- Zhao K, Luo H, Yuan Z, Xu D, Du Y, Zhang S, Hao Y, Wu Y, Huang J, Wang Y, Jiang R (2021). Identification of close relationship between atmospheric oxidation and ozone formation regimes in a photochemically active region. *Journal of Environmental Sciences-China*, 102: 373–383
- Zhu J, Wang S, Wang H, Jing S, Lou S, Saiz-Lopez A, Zhou B (2020). Observationally constrained modeling of atmospheric oxidation capacity and photochemical reactivity in Shanghai, China. *Atmospheric Chemistry and Physics*, 20(3): 1217–1232
- Zhu S, Poetzschner J, Shen J, Wang S, Wang P, Zhang H (2021). Comprehensive insights into O<sub>3</sub> changes during the COVID-19 from O<sub>3</sub> formation regime and atmospheric oxidation capacity. *Geophysical Research Letters*, 48(10): e2021GL093668